Computational model for coupled electron-photon transport in two dimensions

R. P. Datta,* S. D. Altekar, and A. K. Ray
Physics Department, P.O. Box 19059, University of Texas at Arlington, Arlington, Texas 76019

J. E. Morel
Los Alamos National Laboratory, Los Alamos, New Mexico 87545
(Received 23 July 1993; revised manuscript received 18 March 1996)

We have developed a method to perform coupled electron-photon calculations in two spatial dimensions using a partial coupling scheme in which electrons produce photons but photons do not produce electrons. A spatial characteristic scheme is used in conjunction with a second order differencing scheme in energy. The multigroup Legendre cross sections are calculated using the cross section generating code CEPXS, which models a large number of electron interactions including elastic scattering from nuclei, inelastic scattering from collisions with atomic electrons, and radiative scattering from nuclei, and photon interactions such as Compton incoherent scattering, photoelectric absorption, and pair interaction. A two-dimensional calculation performed to simulate results from an experiment in which energy deposition depends only on the depth inside the medium compares very favorably with experimental data. Energy deposition profiles are also obtained for monoenergetic electron sources isotropically incident on aluminum and are compared with TIGER Monte Carlo calculations. Agreement between the two sets of calculations is found to be excellent. In summary, we conclude that our computational model is capable of providing very good results for energy deposition due to an incident source of electrons in two-dimensional rectangular geometry. [S1063-651X(96)10006-4]

PACS number(s): 02.70.−c, 95.30.Jx

I. INTRODUCTION

Electron transport in metals and semiconductors has been of considerable interest for a long time [1–3]. Theoretical studies have usually concentrated on analytical and computational solutions of the Boltzmann transport equation [4,5]. The computational methods can be classified principally into two categories, namely the Monte Carlo methods [6–11] which are statistical in nature and deterministic methods of which the method of discrete ordinates [12–15] has been most widely used. The standard numerical technique for performing coupled electron photon transport calculations is the condensed history Monte Carlo method originally developed by Berger [6] and has been used in codes like ETRAN [8] and the ITS (integrated Tiger series) [16]. These codes have been used to carry out a variety of calculations for a number of quantities of physical interest such as transmission coefficients for slab targets, energy spectra transmitted through slab targets, angular distribution of electrons transmitted through slab targets, reflection coefficients for semi-infinite targets, energy deposition as a function of depth, and detector response functions, and good agreement between calculated values and experimental data has been obtained. While Monte Carlo treatments of electron transport are certainly widespread and well suited in complex geometries, they can be time consuming and expensive. An efficient and alternative deterministic method such as discrete ordinates would be very beneficial in simple geometries. In this paper we concentrate on the method of discrete ordinates to obtain the energy deposition in slab targets (plane parallel geometry) in two spatial dimensions.

The method of discrete ordinates (S_N) has been used successfully in neutral particle applications [17–19]. However, direct application to charged particle transport is difficult due to nonlocal Coulomb interaction. The electron Boltzmann transport equation (BTE) is not amenable to a standard multigroup approximation in energy. This is because an accurate multigroup representation of the collisional cross section for electrons is impractical. Since the inelastic cross section increases rapidly as energy loss becomes small, an accurate multigroup representation would require a rather large number of narrow width groups which would make such a discrete ordinates calculation very expensive. This is particularly true in multidimensional calculations. Small mean free paths and highly anisotropic scattering have also contributed to the problem of efficient studies of charged particle transport. Despite such problems, many authors have studied the problem of electron transport in one spatial dimension using the method of discrete ordinates. The multigroup diffusion method of Corman *et al.* [20], the moments technique of Haldy and Ligaou [21], the LSN method of Antal and Lee [22], and the integral tracking technique of Moses [23] are some well-known methods of one-dimensional electron transport. Melhorn and Duderstadt [24] modified the TIMEX [25] code to provide time-dependent solutions in one-dimensional slab and spherical geometries. Morel [26] developed a method for using standard discrete ordinates neutron transport codes to perform Fokker-Planck calculations in one-dimensional slab and spherical geometries. It is shown that energy-angle integrated quantities such as energy and charge deposition profiles can be accurately and efficiently calculated for electrons. Wienke [27–29] has developed a semianalytical technique of inverting the Boltzmann trans-

*Permanent address: S. N. Bose National Center for Basic Sciences, Salt Lake, Calcutta, 700064, India.

port equation using exponential differencing techniques. In two dimensions, Filippone *et al.* [30] have solved the Spencer-Lewis equation using finite differencing of the spatial variable. The first application of the discrete ordinates method to coupled electron-photon transport calculations was made by Bartine *et al.* [31]. However, their results were not particularly encouraging as a large number of groups had to be used to obtain accurate results and difficulties were encountered in problems with high-Z materials. In recent years Lorence *et al.* [32] has applied the S_N method to coupled electron photon transport in one dimension. In particular, they have shown that their S_N method is as accurate as the condensed-history Monte Carlo method. The reduction in computing times of from one to two orders of magnitude is possible. In their calculations, quantities integrated over energy and angle, such as energy and charge deposition profiles, converged as a function of the number of energy groups at a much faster rate than the differential spectra. This adjoint coupled-electron-photon method is capable of performing calculations, which are not possible with continuous energy Monte Carlo codes. Specifically, in connection with this work, Lorence *et al.* [32] developed the coupled electron-photon multigroup cross-section generation code CEPXS and a one-dimensional coupled electron-photon discrete ordinates code package ONELD [33–35]. CEPXS is a cross-section generating code. The cross-section data it produces are the multigroup-Legendre expansion coefficients of coupled electron-photon cross sections. ONELD is a general Boltzmann discrete ordinates transport code. We will return to a discussion of CEPXS later in this manuscript. Finally, a one-dimensional electron transport solver, based on a streaming ray (SR) solution to the Spencer-Lewis equation, has been developed by Filippone *et al.* [36]. The solver includes several special numerical techniques such as an efficient routine for simulating energy loss straggling, use of extended-transport-corrected and Fokker-Planck equivalent cross sections, a discrete transport correction, and the method of numerical shoves and countershoves. A characteristic line in the SR model lies in the x-s plane, where x is the spatial variable and s is a path length variable directly related to the energy variable. This is in contrast to the multigroup S_N model where electron transport takes place at fixed energy and energy loss is modeled through discrete jumps to lower groups. The model used in our two-dimensional electron transport work [37–39], is basically a multigroup S_N model as opposed to the SR model in which the electron loses energy continuously. A characteristic line in our two-dimensional model lies in the x-y plane where both x and y are spatial variables and none of them is related to the energy.

The purpose of this paper is to study the problem of coupled electron photon transport in two dimensions due to an incident source of electrons. Specifically, we have developed a technique that can be considered a two-dimensional generalization of the one-dimensional CEPXS/ONELD method of Lorence *et al.* [40,41]. Our main consideration has been to develop a two-dimensional technique compatible with the CEPXS multigroup cross-section data generation code. CEPXS includes all of the coupled electron-photon interaction physics treated in production Monte Carlo codes such as those in the ITS system [16]. It is advantageous to use the CEPXS data not only because we obtain the most complete and accurate interaction physics, but also because comparisons of our deterministic solutions with Monte Carlo solutions will reflect only differences in numerical accuracy as opposed to differences in both interaction physics and numerical accuracy. In the following section, the outlines of the theory are presented, followed by results and conclusions in Sec. III.

II. THEORY

We first write the coupled electron-photon Boltzmann transport equation in two-dimensional x-y geometry as

$$\mu\frac{\partial f_e}{\partial x}+\eta\frac{\partial f_e}{\partial y}+\sigma_{te}f_e=\int\int dE'd\Omega' f_e(x,y,E',\Omega')\sigma_{e\text{-}e}(E'\rightarrow E,\Omega'\Omega)+\int\int dE'd\Omega' f_p(x,y,E',\Omega')\sigma_{p\text{-}e}(E'\rightarrow E,\Omega'\Omega)+Q_e(x,y,E,\Omega), \tag{1}$$

$$\mu\frac{\partial f_p}{\partial x}+\eta\frac{\partial f_p}{\partial y}+\sigma_{tp}f_p=\int\int dE'd\Omega' f_p(x,y,E',\Omega')\sigma_{p\text{-}p}(E'\rightarrow E,\Omega'\Omega)+\int\int dE'd\Omega' f_e(x,y,E',\Omega')\sigma_{e\text{-}p}(E'\rightarrow E,\Omega'\Omega)+Q_p(x,y,E,\Omega), \tag{2}$$

in which f is the particle flux (number density of particles times their speed) defined such that $fdVdEd\Omega$ is the flux of particles in the volume element dV about r, in the element of solid angle $d\Omega$ about Ω and in the energy range dE about E. Similarly $QdVdEd\Omega$ is the number of particles in the same element of phase space emitted by sources independent of f. The subscripts e and p stand for electron and photon, respectively. The macroscopic total interaction cross section is denoted by σ_{te} for electrons and σ_{tp} for photons. The cumulative electron to electron differential scattering cross section is denoted by $\sigma_{e\text{-}e}$, the cumulative photon to electron differential scattering cross section is denoted by $\sigma_{p\text{-}e}$, the cumulative photon to photon differential scattering cross section is denoted by $\sigma_{p\text{-}p}$, and the cumulative electron to photon differential scattering cross section is denoted by $\sigma_{e\text{-}p}$. All of these cross sections may be dependent on the spatial

variables x and y but in our case we have assumed no spatial dependence of the total interaction cross section and the scattering cross section.

Equations (1) and (2) describe the actual physical situation in which electrons can give rise to photons and photons can give rise to electrons. However, for certain types of problems, it is not necessary to consider full coupling between electrons and photons. We have thus implemented a partial coupling scheme in our computational model in which photons are produced from electrons but the production of electrons from photons is not accounted for. Such a partial coupling scheme has been used by Lorence *et al.* [32] in one-dimensional applications and noted to be of particular usefulness in shielding calculations such as those pertaining to the shielding of spacecraft electronics from geomagnetically trapped electrons. The partial coupling scheme as described above amounts to setting the photon to electron scattering cross section $\sigma_{p\text{-}e}$ equal to zero. Then the electron flux in Eq. (1) f_e can be solved without reference to the photon flux f_p. However, the photon cross interactions associated with electron production can still contribute to the total photon cross section. The energy which would have gone into the photon produced electrons is considered to be deposited where the photon interaction occurs. If the energy of the incident electron is greater than the critical energy given by $800/Z$ in MeV [42], i.e., the energy below which collisional losses predominate, the dominant physical interaction of the bremsstrahlung produced photons in pair interaction and the above approximation will not be valid. In the description that follows we omit the subscripts e and p to denote electrons and photons. It is understood that quantities without a subscript e or p can stand for either electrons or photons. The reduction of the Boltzmann transport equation to a discretized form suitable for computation is similar for electrons and photons. This has been presented before for electrons [38], however, for the sake of completeness, we present it again to discuss the full nature of coupling between electrons and photons.

In our work, the scattering transfer probability (electrons and photons) is assumed to be represented by a Legendre polynomial expansion of the form

$$\sigma_s(E'\rightarrow E,\mu_0)=\sum_{n=0}^{\mathrm{ISCT}}(2n+1)P_n(\mu_0)\sigma_s(E'\rightarrow E), \quad (3)$$

where

$$\mu_0=\Omega\Omega'=\mu\mu'+(1-\mu^2)^{1/2}+(1-\mu'^2)^{1/2}\cos(\varphi-\varphi')$$

and ISCT is the order of scattering.

Using cross-section expansion and the addition theorem for Legendre polynomials, we now write (1) as

$$\mu\frac{\partial f}{\partial x}+\eta\frac{\partial f}{\partial y}+\sigma_t f=\int_0^\infty dE'\sum_{n=0}^{\infty}(2n+1)\sigma_{sn}(E'\rightarrow E)\times\sum_{k=0}^{n}R_n^k(\mu,\phi)f_n^k+Q_{\mathrm{ext}}(x,y,E,\Omega). \quad (4)$$

The functions R_n^k are defined by

$$R_n^k=\left[\frac{(2-\delta_{k0})(n-k)!}{(n+k)!}\right]^{1/2}P_n^k(\mu_0)\cos(k\phi), \quad (5)$$

where P_n^k are the associated Legendre polynomials. If the angular flux f is expanded in a series of these functions, then the f_k^n denote the expansion coefficients and are given by

$$f_k^n=\int_{-1}^{1}d\mu\int_0^{\pi}d\phi R_k^n f/2. \quad (6)$$

These coefficients are calculated by using the fully symmetric quadrature sets given in Lewis and Miller [15] and Lathrop and Carlson [43]. At this point, we set $Q_{\mathrm{ext}}(x,y,E,\Omega)=0$ implying the absence of external sources.

The multigroup equations are now obtained by dividing the energy domain of interest into IGP intervals (referred to as groups) of width ΔE_g and integrating Eq. (4) over a particular energy group. The final form of the space, energy, and angle discretized coupled electron-photon transport equations in the partial coupling approximation is given by

$$\mu\frac{\partial f_g^e}{\partial x}+\eta\frac{\partial f_g^e}{\partial y}+\sigma_{tg}^e f_g^e=\sum_{h=1}^{\mathrm{IGP}}\sum_{n=0}^{\mathrm{ISCT}}(2n+1)\sigma_{snh\rightarrow g}^{e\text{-}e}\sum_{k=0}^{n}R_{nm}^k\sum_{m=1}^{\mathrm{MT}}w_m R_n^k(\mu_m,\phi_m)f_{gijm}^e \quad (7)$$

and

$$\mu\frac{\partial f_g^p}{\partial x}+\eta\frac{\partial f_g^p}{\partial y}+\sigma_{tg}^p f_g^p=\sum_{h=1}^{\mathrm{IGP}}\sum_{n=0}^{\mathrm{ISCT}}(2n+1)\sigma_{snh\rightarrow g}^{p\text{-}p}\sum_{k=0}^{n}R_{nm}^k\sum_{m=1}^{\mathrm{MT}}w_m R_n^k(\mu_m,\phi_m)f_{gijm}^p+\sum_{h=1}^{\mathrm{IGP}}\sum_{n=0}^{\mathrm{ISCT}}(2n+1)\sigma_{snh\rightarrow g}^{e\text{-}p}\sum_{k=0}^{n}R_{nm}^k\sum_{m=1}^{\mathrm{MT}}w_m R_n^k(\mu_m,\phi_m)f_{gijm}^e. \quad (8)$$

We now describe the solution to the within group equations. Once again we suppress the subscripts e and p and note that the procedure is analogous for electrons and photons. Omitting the group subscript g, the within group equation in the discrete ordinates form is

$$\mu_n \frac{\partial f_n(x,y)}{\partial x} + \eta_n \frac{\partial f_n(x,y)}{\partial y} + \sigma_n f_n(x,y) = q(x,y,\eta_n,\mu_n), \tag{9}$$

where $q(x,y,\eta_n,\mu_n)$ is the within group scattering source for a mesh point (x,y) and discrete ordinate direction (μ_n,η_n).

In simpler notation we write the above equation as

$$a\frac{\partial f_n}{\partial x} + b\frac{\partial f_n}{\partial y} + c f_n = d(x,y), \tag{10}$$

where $a=\mu_n$, $b=\eta_n$, $c=\sigma(x,y)$, $d(x,y)=q(x,y,\mu_n,\eta_n)$, and the cross section is assumed to be constant. We have used the method of characteristics [38] and the final differencing scheme is given by

$$f_n(x_i,\xi(x_i)) = \exp\left(-\frac{c}{a}x_i\right)\left[\frac{1}{a}\int_{x_{i-1}}^{x_i} \overline{d}(s,\xi(s))\exp\left(\frac{c}{a}s\right)ds + f_n(x_{i-1},\xi(x_{i-1}))\exp\left(\frac{c}{a}x_{i-1}\right)\right]. \tag{11}$$

Therefore given the angular flux f_n at $(x_{i-1},\xi(x_{i-1}))$ we can calculate f_n at $(x_i,\xi(x_i))$, where $y=\xi(x)$ is a characteristic, i.e., particle trajectory.

The spatial interpolation scheme will depend on the direction of particle travel which can be in four different directions given by the following cases. (a) Travel from left to right and from bottom to top. (b) Travel from left to right and from top to bottom. (c) Travel from right to left and from bottom to top. (d) Travel from right to left and from top to bottom. Here we only discuss briefly the first case.

Consider a typical two-dimensional mesh cell as shown in Fig. 1. The direction of travel is from left to right and from bottom to top characterized by $\mu>0$ and $\eta>0$. The angular flux $f_n(x_i,y_i)$ is written as $N(i,j)$ for a particular direction (μ,η) where we have omitted the subscript n. The source $d(x,\xi)$ is assumed to be constant over the mesh cell and is denoted by S. The exponential term inside the integral is treated analytically and the angular flux at the point where the characteristic drawn through the right top corner intersects the cell boundary (left vertical if ρ is less than 1 and bottom horizontal if ρ is greater than 1) is denoted by $\tilde{N}$ and ρ is defined as

$$\rho = \left|\frac{\eta\Delta x}{\mu\Delta y}\right|. \tag{12}$$

Equation (11) then can be written as

$$N(i+1,j+1) = \tilde{N}\exp\left(-\frac{\sigma\Delta x}{|\mu|}\right) + \frac{S}{\sigma}\left[1-\exp\left(-\frac{\sigma\Delta x}{|\mu|}\right)\right]. \tag{13}$$

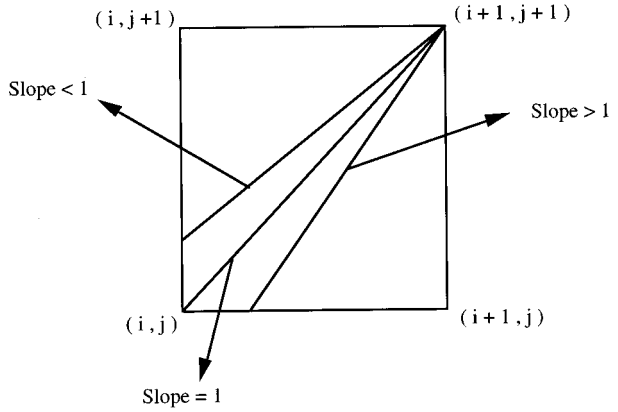

FIG. 1. Interpolation scheme based on the slope of the characteristics.

The value of $\tilde{N}$ is given by

$$\tilde{N} = \rho N(i,j) + (1-\rho)N(i,j+1), \quad \rho<1 \tag{14}$$

and

$$\tilde{N} = 1/\rho N(i,j) + (1-1/\rho)N(i,j+1), \quad \rho>1. \tag{15}$$

Thus, if the characteristic drawn through the right upper corner of the cell intersects the left vertical boundary, we interpolate between the left upper and the left lower corners. If the same characteristic intersects the bottom horizontal boundary, we interpolate between the left lower and the right lower corners.

Now, the two-dimensional differencing scheme that we use must satisfy the conservation relation for particles entering and leaving the mesh cell together with the sources inside the cell. For $\mu,\eta>0$, the two-dimensional linear Boltzmann equation written in a conservation form over a two-dimensional rectangular mesh cell is

$$\frac{\mu(N_{i+1}-N_i)}{\Delta x} + \frac{\eta(N_{j+1}-N_j)}{\Delta y} + \sigma N = S, \tag{16}$$

where N denotes the cell average flux over the two-dimensional mesh cell and the other quantities are defined as

$$2N_i = N(i,j+1) + N(i,j), \tag{17}$$

$$2N_{i+1} = N(i+1,j+1) + N(i+1,j), \tag{18}$$

$$2N_j = N(i,j) + N(i+1,j), \tag{19}$$

$$2N_{j+1} = N(i,j+1) + N(i+1,j+1). \tag{20}$$

Substituting for N_i, N_{i+1}, N_j, and N_{j+1} from Eqs. (17)–(20) into Eq. (16) we get

$$\mu\frac{N(i+1,j+1)+N(i+1,j)-N(i,j+1)-N(i,j)}{2\Delta x}+\eta\frac{N(i+1,j+1)+N(i,j+1)-N(i+1,j)-N(i,j)}{2\Delta y}+\sigma N=S. \quad (21)$$

We now substitute for $N(i+1,j+1)$ from Eq. (13) in Eq. (21) and solve for N which gives

$$N=\frac{S}{\sigma}-\frac{\mu}{2\sigma\Delta x}\left[\widetilde{N}\exp\left(-\frac{\sigma\Delta x}{|\mu|}\right)+\frac{S}{\sigma}1-\exp\left(-\frac{\sigma\Delta x}{|\mu|}\right)+N(i+1,j)-N(i,j+1)-N(i,j)\right]$$
$$-\frac{\eta}{2\sigma\Delta y}\left[\widetilde{N}\exp\left(-\frac{\sigma\Delta x}{|\mu|}\right)+\frac{S}{\sigma}1-\exp\left(-\frac{\sigma\Delta x}{|\mu|}\right)+N(i,j+1)-N(i,j)-N(i+1,j)\right]. \quad (22)$$

In this case since $N(i,j)$, $N(i,j+1)$, and $N(i+1,j)$ are known, Eq. (13) can be used to calculate the flux $N(i+1,j+1)$. After that we use Eq. (22) to calculate the cell average flux that satisfies the conservation relation for particles entering and leaving the mesh cell together with sources inside the cell. Fluxes calculated using this difference scheme will therefore conserve particles due to spatial differencing. We note that [22] does not guarantee a positive cell average flux. However, in our calculations, negative fluxes were not significant and no fixup of any kind was used.

There are two ways to represent the restricted CSD approximation [44] in discrete ordinates codes. The restricted CSD operator could be differenced directly into the code [31]. The approach taken in our calculations is the approach devised by Morel [26] in which ''pseudo'' multigroup Legendre cross sections are devised to represent the different form of the restricted CSD operator. These CSD cross sections do not have a microscopic counterpart but they enable a standard multigroup code to obtain real physical solutions to the underlying Boltzmann-CSD equations. The multigroup cross sections used in our calculations are generated by the cross section generating code CEPXS [33–35]. The different electron cross sections generated by the code are as follows.

(i) Elastic scattering. The cross section data of Riley *et al.* [45] are used at nonrelativistic energies. The Mott cross section with Moliere screening is used at relativistic energies [6,46]. The extended transport correction [47] is applied to these elastic scattering cross sections to make them amenable to representation by a low-order Legendre expansion.

(ii) Inelastic scattering. The Moller cross section [46] is used for large energy loss collisions. For other collisions, the restricted CSD (continuous slowing down) approximation is used. In this approximation, the restricted collisional stopping power specifies the energy loss of the electron per path length due to small energy loss collisions only. This is calculated as the difference between the total collisional stopping power and that portion of the total collisional stopping power that is due to large energy loss collisions. The total collisional stopping power [48] is tabulated at discrete energies for all elements in the set of electron data called DATAPAC [8].

(iii) Knock-on production. Knock-on electrons are defined to be the least energetic electrons that emerge following an inelastic collision. The Moller cross section [46] is used to determine the production of knock-on electrons with energies to the cutoff energy.

(iv) Radiative energy loss. The bremsstrahlung cross section is based on a formulation by Berger and Seltzer [49], involving Born approximation cross sections described by Koch and Motz [50]. This cross section is used to describe the slowing down of an electron by radiative emission that results in large energy losses. For small energy loss radiative events the restricted CSD approximation is used, which specifies the energy loss of the electron per path length due to radiative emission in which the energy loss is small. Once again it is calculated as a difference between the total radiative stopping power [48] tabulated at discrete energies for all elements in DATAPAC [8], and that portion of the total radiative stopping power that is due to large energy loss radiative events.

(v) Impact ionization. The impact ionizations in CEPXS are not correlated with inelastic collisions. They are used solely to determine the production of relaxation radiation. The energy of the relaxation particle is less than or equal to the binding energy of the shell that is ionized. The Gryzinski [51] impact ionization cross sections are used for the K, $L1$, $L2$, $L3$, and M shells.

The different photon cross sections generated by the code are as follows.

(i) Compton incoherent scattering. The Klein-Nishina cross section [52] is used for Compton incoherent scattering of photons with atomic electrons. This cross section was derived for scattering from free or unbound electrons. When the photon energy is on the order of the atomic binding energies this assumption is not valid. However, photoelectric absorption dominates incoherent scattering at such energies.

(ii) Photoelectric absorption. An incident photon cannot be totally absorbed by a free electron. However, total absorption can take place if the electron is initially bound in an atom. The tightly bound electrons have the greatest probability of absorbing a photon. About 80% of the photoelectric absorption process takes place in the K shell if the incident photon energy clearly exceeds the K-shell binding energy. The Biggs-Lighthill [53] cross sections are used for photoelectric absorption.

(iii) Pair interaction. The photon is completely absorbed in this process and in its place appears a positron-electron pair whose total energy is equal to the energy of the incident photon. The Biggs-Lighthill [49] cross sections are used for the absorption of photons by pair interaction.

III. COMPUTATIONAL DETAILS AND RESULTS

In this section we shall discuss the computational details and results of our calculations. The quantity of interest is the

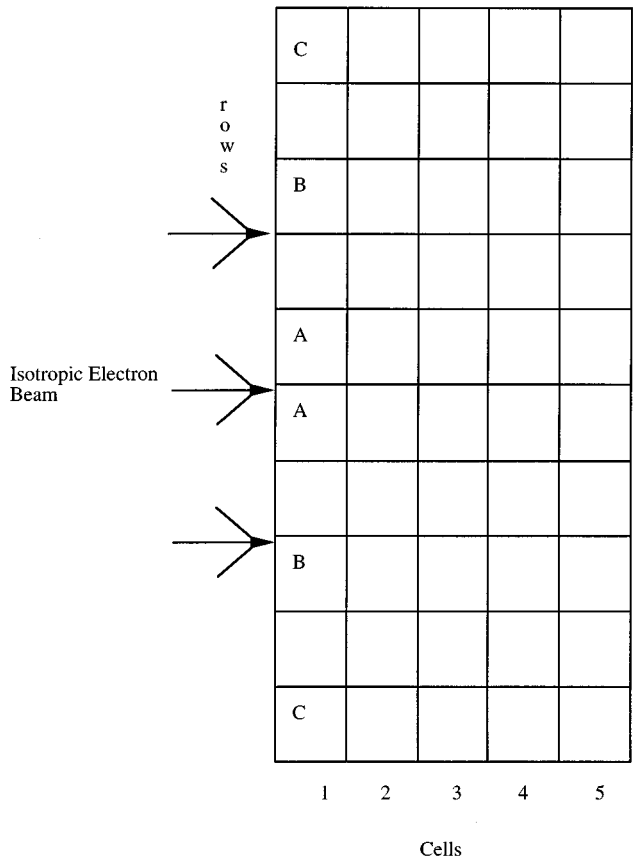

FIG. 2. Mesh cells for energy deposition calculation.

energy deposition which is calculated using the formula

$$E_{\mathrm{dep}}(x,y)=\sum_{g=1}^{\mathrm{IGP}} N_g(x,y)\Sigma_g, \tag{23}$$

where $E_{\mathrm{dep}}(x,y)$ is the energy deposited in a mesh cell which has (x,y) as its left lower corner point, N_g denotes the cell average multigroup scalar flux for electrons or photons (obtained by summing the multigroup angular flux over all directions) for the same spatial mesh cell, and Σ_g is the energy deposition cross section for electrons or photons, which is defined as the net energy deposited in the medium due to interactions of particles in a group per unit path length and has units of energy per distance. IGP is the total number of groups. The total energy deposition is obtained as a sum of the energy deposited due to electrons and photons.

TABLE I. Comparison of calculated and experimentally measured dose behind aluminum slab shields irradiated by monoenergetic, isotropic electron beams.

Incident energy MeV	Thickness mil	Expt. dose MeV/gm	Calculated dose MeV/gm
1	30	1.762 2±0.176 22	1.754
2	30	2.627 3±0.256 32	2.572
3	30	2.707 4±0.272 34	2.931
4	30	2.387 0±0.240 30	2.453
1	60	0.125 11±0.125 11	0.659
2	60	1.890 4±0.192 24	1.954
3	60	2.483 1±0.256 32	2.543
4	60	2.178 7±0.224 28	2.404

The computations are performed on a two-dimensional rectangle having 20 divisions in the x direction and 40 divisions in the y direction as shown in Fig. 2. In the calculations presented in this paper we choose the x length of the rectangle to be half the y length in all cases. Thus the mesh cells in our calculations are squares. However, it should be pointed out that this method can be applied to rectangular mesh cells as well. All calculations are performed using the fully symmetric Galerkin quadrature sets given by Morel [54]. As is known, proper treatment of the continuous-slowing-down operator represented by the CEPXS data requires an exact treatment of truncated δ-function cross-section expansions. In one-dimensional calculations standard Gauss quadratures properly treat such expansions, but there exists no two-dimensional (or three-dimensional) quadratures which do so. The special Galerkin quadrature method always treats truncated δ-function scattering expansions correctly in all dimensions. We use Galerkin quadratures in all of our calculations in order to ensure proper treatment of the continuous-slowing-down term. To our knowledge, Galerkin quadratures have not previously been used in multidimensional coupled electron-photon transport calculations. Also, as pointed out in the Introduction, the number of energy groups can be rather large to accurately account for electrons

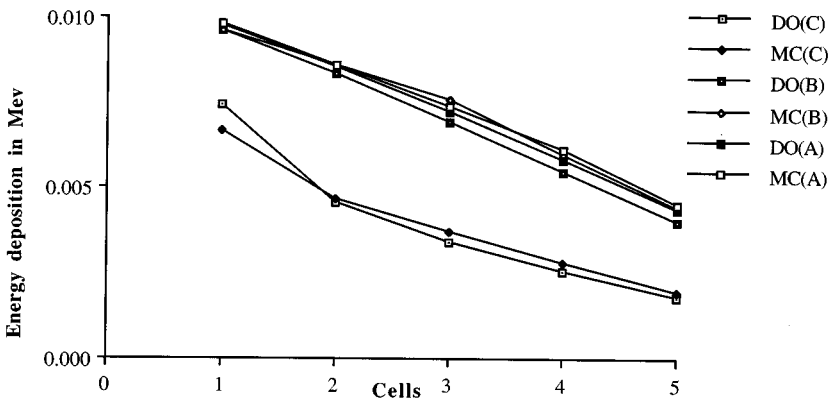

FIG. 3. Energy deposition for 1 MeV isotropic electrons incident on an aluminum slab of dimension 0.2×0.4 cm.

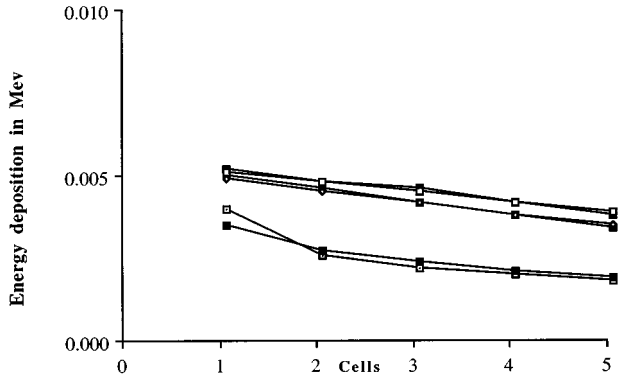

FIG. 4. Energy deposition for 1 MeV isotropic electrons incident on an aluminum slab of dimension 0.1×0.2 cm.

slowing down. However, by dividing the energy loss processes into large and small energy loss collisions (restricted stopping power formalism), it is possible to account for the energy loss in a pseudomultigroup approach by using a considerably lower number of energy groups. This approach coupled with a second order difference scheme in energy has proved to be highly accurate in one-dimensional applications [32–35]. We, therefore, chose to apply the same technique in our two-dimensional calculations.

To further validate our results, we note that the experimentally measured dose by Van Guyten [55] behind aluminum slabs of different thicknesses irradiated by monoenergetic isotropic electron beams of different energies was reported by Seltzer [56]. To simulate this experimental setup we consider an isotropic beam of electrons incident on the left boundary of the slab (Fig. 2). Table I gives the calculated and experimentally measured doses for aluminum slabs of different thicknesses for isotropically incident monoenergetic electron sources. These calculations are performed using matrix quadrature sets of order 12 with the cross-section expansion through order 12. The number of electron groups is 40 and the number of photon groups is 40 with the cutoff energy in each case being 50 keV. All the groups are chosen to be uniform implying that the group widths are constant. The x thickness of the slab is set at 30 ml and 60 ml, and the corresponding y thicknesses at 60 and 120 ml, respectively, where 1 ml $=0.006\,86$ gm/cm^2. The unit of length gm/cm^2 is obtained by multiplying the conventional unit cm by the density of the medium and is the *de facto* standard in the field of electron transport. As can be observed from Table I, the calculated values indeed compare very well with the experimentally measured values over a wide range of incident energies and slab thicknesses, our values lying within the experimental uncertainties in all cases except one. The only exception is the case of 1 MeV electrons incident on a 60-ml-thick slab. However, the uncertainty in the experimental value of this case is 100%. The CSDA range for a 1-MeV electron is 0.5542 gm/cm^2, which is very close to the thickness 60 ml $=$ 0.4116 gm/cm^2 of the slab. Thus the discrepancy can be attributed to the fact that the thickness is rather close to the CSDA range for the particular energy.

Having thus established the fact that our partial coupling scheme is a valid computational tool for calculating energy deposition, we now focus our attention on an isotropic source incident on the left face of the slab. Once again the x length of the slab is taken to be half of the y length, the order of the discrete ordinates calculations is 12, and the cross-section expansions are through order 12; there are 40 electron groups and 40 photon groups, the cutoff energy being 50 keV. Figures 3–5 present our results along with the results obtained from the ITS code [16] run at Sandia National Laboratory [57]. Figure 3 shows the energy deposition for rows A, B, and C for cells 1 through 5 for a 1-MeV monoenergetic isotropic electron source incident on a slab of aluminum 0.2 by 0.4 cm in dimension. Figure 4 shows the energy deposition for the same case as in Fig. 3 but for a 0.1 by 0.2 cm slab. The energy deposition due to 5-MeV electrons on a 0.6 by 1.2 cm slab is shown in Fig. 5. From the graphs it is seen that our results compare very well with the Monte Carlo results. The dose for all the rows falls off as we move away from the source into the medium. However, this drop is steeper when the dimension of the slab is comparable with the CSDA range of the particular incident energy. Also, the agreement with Monte Carlo results is generally more favorable when the dimension of the slab is less than the CSDA range which is 0.2 cm for 1 MeV and 1.2 cm for 5 MeV. However, the general pattern of the dose profile is very clear. The energy deposited in row C, which denotes the zones at the upper and lower boundaries of the slab, are significantly less than the energy deposited in rows A and B, which are closer to the center. Although the depositions for

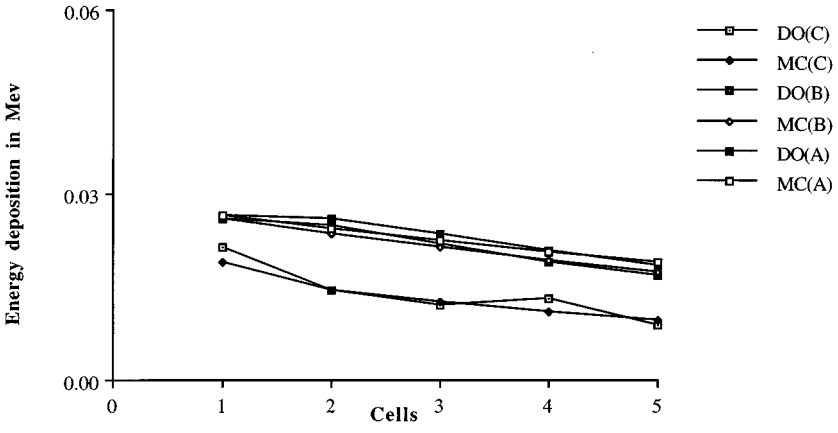

FIG. 5. Energy deposition for 5 MeV isotropic electrons incident on an aluminum slab of dimension 0.6×1.2 cm.

row A and row B are very close, row B is lower than row A. Basically, this implies that with isotropic sources, energy deposition decreases as we move away from the center of the slab. For thicker slabs, we expect finer meshes will be necessary to obtain reliable results. Finally, although the ONELD transport code uses a linear-discontinuous (LD) spatial discretization for coupled electron-photon transport calculations, we have chosen to use a simpler step-characteristic (SC) method in our two-dimensional calculations. Step-characteristic methods have been used previously by Filippone *et al.* [36] in one-dimensional electron transport calculations. Our two-dimensional SC method has one unknown per spatial cell per angle per group and is second-order accurate, whereas the two-dimensional LD method has three unknowns per spatial cell per angle per group and is third-order accurate. Since the main thrust of our work is to develop the first two-dimensional coupled electron-photon transport calculations with Galerkin quadrature and the CEPXS cross-section data, the spatial differencing scheme that we use is not particularly important as long as it is reasonably effective. However, we do intend to pursue more accurate step-characteristic methods [58,59] in our future work.

ACKNOWLEDGMENTS

The authors gratefully acknowledge partial support from State of Texas Advanced Technology Program (Grant No. 003656-120) and Cray Research. The authors also wish to thank Dr. L. Lorence and Dr. R. Kensek at Sandia National Laboratory for making Monte Carlo results available to us to compare with our discrete ordinates calculations. Computational support from the University of Texas Center for High Performance Computing is also gratefully acknowledged.

[1] L. V. Spencer, Phys. Rev. **98**, 1507 (1955).
[2] I. P. Shkarofsky, T. W. Johnston, and M. P. Bachynski, *Particle Kinetics in Plasmas* (Addison Wesley, Reading, MA, 1976).
[3] B. R. Nag, *Electron Transport in Compound Semiconductors* (Springer-Verlag, New York, 1980).
[4] L. Boltzmann, *Lectures on Gas Theory* (University of California Press, Berkeley, 1964).
[5] C. Cercignani, *The Boltzmann Equation and Its Applications* (Springer-Verlag, New York, 1988).
[6] M. J. Berger, in *Methods in Computational Physics*, edited by B. Adler (Academic, New York, 1969), Vol. 1, p. 135.
[7] M. J. Berger and S. M. Seltzer, NASA Report No. SP-71 437, 1965.
[8] M. J. Berger and S. M. Seltzer, Radiation Shielding Information Report No. CCC-107, 1968.
[9] R. N. Hamm, J. E. Turner, H. A. Wright, and R. H. Ritchie, IEEE Trans. Nucl. Sci. **Ns-26**, 4892 (1979).
[10] R. Shimizu, J. Ikuta, and K. Murata, J. Appl. Phys. **43**, 4233 (1972).
[11] J. A. Halbleib, Sr. and W. Vandevender, Sandia National Laboratories Report No. Sand 74-0030 (1975).
[12] B. G. Carlson and K. D. Lathrop, in *Computing Methods in Reactor Physics*, edited by H. Greenspan, C. N. Kelber, and D. Okrent (Gordon & Breach, New York, 1968), p. 171.
[13] G. I. Bell and S. Glasstone, *Nuclear Reactor Theory* (Van Nostrand Reinhold, Reading, MA, 1970).
[14] J. J. Duderstadt and W. R. Martin, *Transport Theory* (Wiley, New York, 1979).
[15] E. E. Lewis and W. F. Miller, Jr., *Computational Methods of Neutron Transport* (Wiley, New York, 1984).
[16] J. A. Halbleib and T. A. Melhorn, Report No. SAND84-0573, Sandia National Laboratory (1984).
[17] T. R. Hill, Los Alamos National Lab. Report No. LA-5990 MS, 1975.
[18] R. E. Alcouffe, E. W. Larsen, W. F. Miller, and B. R. Wienke, Nucl. Sci. Eng. **71**, 111 (1979).
[19] E. W. Larsen, Nucl. Sci. Eng. **82**, 64 (1982).
[20] E. G. Corman, W. E. Loewe, G. E. Cooper, and A. M. Winslow, Nucl. Fusion **15**, 377 (1975).
[21] P. A. Haldy and J. Ligaou, Nucl. Fusion **17**, 1225 (1977).
[22] M. J. Antal and C. J. Lee, J. Comp. Phys. **20**, 298 (1976).
[23] G. A. Moses, Nucl. Sci. Eng. **64**, 49 (1977).
[24] T. A. Melhorn and J. J. Duderstadt, J. Comp. Phys. **38**, 86 (1980).
[25] T. R. Hill and W. H. Reed, Los Alamos National Lab. Report No. LA-6201-MS (1976).
[26] J. E. Morel, Nucl. Sci. Eng. **79**, 340 (1981).
[27] B. R. Wienke, J. Quant. Spectrosc. Radiat. Trans. **28**, 311 (1982).
[28] B. R. Wienke, Nucl. Tech./Fusion **4**, 426 (1983).
[29] B. R. Wienke, J. Comp. Phys. **51**, 208 (1983).
[30] W. L. Filippone, S. Woolf, and J. C. Garth, IEEE Trans. Nucl. Sci. **NS-34**, 1564 (1987).
[31] D. E. Bartine, R. G. Alsmiller, Jr., F. R. Mynatt, W. W. Engle, Jr., and J. Barish, Nucl. Sci. Eng. **48**, 159 (1979).
[32] L. J. Lorence, Jr., W. E. Nelson, and J. E. Morel, IEEE Trans. Nucl. Sci. **NS-32**, 4416 (1986).
[33] L. J. Lorence, Jr., J. E. Morel, and G. D. Valdez, Sandia National Lab. Report No. SAND89-1661 (1989).
[34] L. J. Lorence, Jr., J. E. Morel, and G. D. Valdez, Sandia National Lab. Report No. SAND89-1685 (1989).
[35] L. J. Lorence, Jr., J. E. Morel, and G. D. Valdez, Sandia National Lab. Report No. SAND89-2211 (1990).
[36] W. L. Filippone, M. S. Smith, S. Woolf, and J. C. Garth, Nucl. Sci. Eng. **95**, 22 (1987).
[37] R. P. Datta, A. S. Hira, A. K. Ray, and B. R. Wienke, Supercomputer **50** (IX-4), 12 (1992).
[38] R. P. Datta, A. K. Ray, and B. R. Wienke, J. Phys. D **26**, 1077 (1993).
[39] R. P. Datta and A. K. Ray, Phys. Status Solidi B **180**, 85 (1993).
[40] R. P. Datta, Ph.D. dissertation, University of Texas at Arlington, 1993.
[41] S. D. Altekar, Ph.D. dissertation, University of Texas at Arlington, 1995.
[42] K. O'Brien, in *Computer Techniques in Radiation Transport and Dosimetry*, edited by R. Nelson and T. M. Jenkins (Plenum, New York, 1980).

[43] K. D. Lathrop and B. G. Carlson, Los Alamos National Lab. Report No. LA-3186 (1964).
[44] J. E. Morel, Nucl. Sci. Eng. **91**, 324 (1985).
[45] M. E. Riley, C. J. Maccallum, and F. Biggs, At. Data Nucl. Data Tables **15**, 443 (1975).
[46] C. D. Zerby and F. L. Keller, Nucl. Sci. Eng. **27**, 190 (1967).
[47] J. E. Morel, Nucl. Sci. Eng. **71**, 64 (1979).
[48] International Commission on Radiation Units and Measurements Report No. 37 (1984).
[49] M. J. Berger and S. M. Seltzer, Phys. Rev. C **2**, 621 (1970).
[50] H. W. Koch and J. W. Motz, Rev. Mod. Phys. **31**, 920 (1959).
[51] M. Gryzinsky, Phys. Rev. **138**, A322 (1965).
[52] P. Marmier and S. Sheldon, *Physics of Nuclei and Particles* (Academic, New York, 1969).
[53] F. Biggs and R. Lighthill, Report No. SC-RR-66-452, Sandia National Laboratories (1969).
[54] J. E. Morel, Nucl. Sci. Eng. **101**, 72 (1989).
[55] O. O. Vanguyten, thesis, University of Maryland (1974).
[56] S. M. Seltzer, IEEE Trans. Nucl. Sci. **NS-26**, 4896 (1979).
[57] L. Lorence and R. Kensek (private communications).
[58] K. D. Lathrop, GA-8746, Gulf General Atomic (1968).
[59] R. E. Alcouffe and E. W. Larsen, Proceeding of the International Topical Meeting of Advances in Mathematical Methods for Solution of Nuclear Engineering Problems, Munich, Germany, 1981 (Fachinformationszentrumenergie, Physik Mathematika, GmbH, Karlsruhe, 1981), Vol. 1, p. 3.